



Spatial Variability of Marine Heatwaves in the Chesapeake Bay

Rachel Wegener¹ · Jacob Wenegrat¹ · Veronica P. Lance² · Skylar Lama^{3,4}

Received: 13 August 2024 / Revised: 18 April 2025 / Accepted: 20 April 2025
© The Author(s) 2025

Abstract

The Chesapeake Bay is the largest estuary in the continental United States. Extreme temperature events, termed marine heatwaves, are impacting this ecologically important zone with increasing frequency. Although marine heatwaves evolve across space and time, a complete spatial picture of marine heatwaves in the Bay is missing. Here, we use satellite sea surface temperature to characterize marine heatwaves in the Chesapeake Bay. We consider three products: NASA MUR, NOAA Geo-Polar, and Copernicus Marine OSTIA, and validate their effectiveness using in situ data from the Chesapeake Bay Program. We find that Geo-Polar SST is the most suitable dataset for marine heatwave analysis in this location, with a root mean squared error of 1.6°C. Marine heatwaves occur on average of 2.3 times per year and last 10.8 days per event. A north-south (along estuary) gradient is identified as a common pattern of spatial variability. Seasonally, summer marine heatwaves are shorter, more frequent, and have a more consistent duration, with an inter-quartile range of 6–11 days (median=8 days). December marine heatwaves have a much larger inter-quartile range of 6–28 days (median=13 days). Marine heatwaves are increasing at a rate of 4 events/year in the upper Bay and 2 events/year in the main stem of the lower Bay. Our analysis suggests that the major observed spatial patterns are a result of long-term warming, not shifts in the spread of the temperature distribution. Overall, the qualitative character of marine heatwaves in the Chesapeake Bay is not changing but they are becoming more frequent.

Keywords Marine heatwaves · Sea surface temperature · Estuary · Chesapeake Bay · Satellite remote sensing

Communicated by Paul A. Montagna.

✉ Rachel Wegener
rwegener@umd.edu

Jacob Wenegrat
wenegrat@umd.edu

Veronica P. Lance
veronica.lance@noaa.gov

Skylar Lama
slama8@gatech.edu

¹ Department of Atmospheric and Oceanic Science, University of Maryland, College Park, 4254 Stadium Drive, College Park, MD 20742, USA

² National Oceanic and Atmospheric Administration (NOAA) National Office of Satellite Data and Information Service, Center for Satellite Applications and Research, and NOAA Coastwatch, 5830 University Research Court, College Park, MD 20740, USA

³ School of Earth and Atmospheric Science, Georgia Institute of Technology, 311 First Dr, Atlanta, GA 30332, USA

⁴ Ocean Science and Engineering, Georgia Institute of Technology, 311 First Dr, Atlanta, GA 30332, USA

Introduction

Anthropogenic activities have warmed the surface ocean, with signs of surface warming going back to at least the mid-1950s (Tyrell, 2011). In addition to increasing average temperatures, prolonged periods of anomalously hot water, termed marine heatwaves (MHW), have been on the rise (Oliver et al., 2019). Extreme temperature events such as MHWs affect marine ecosystems on the individual, population, and community levels (Smith et al., 2023), but ecosystem response can differ based on the characteristics of the MHW such as duration and rate of onset (Smith et al., 2023). These ecosystem impacts translate into socioeconomic impacts. ~~In the US alone~~, economic losses "...exceed US\$800 million in direct losses and in excess of US\$3.1 billion per annum in indirect losses for multiple consecutive years" from MHW events (through October 2022) (Smith et al., 2021). MHWs and their ecological and economic impact are unfortunately part of our warming world.

Efforts to study MHW with satellite imagery have been undertaken for study areas around the world (see: Mohamed et al., 2022; Chatterjee et al., 2022; Huang et al., 2021; Oliver

et al., 2018). Satellite imagery provides a temporally consistent data source over a broad spatial scale, making it a strong data product for the analysis of MHW. While more difficult, past work has also investigated MHW in the coastal ocean. Marin et al. (2021)'s global coastal MHW analysis showed increasing numbers of MHW events, with concentrated increases in hotspots. One of the identified hotspots is the northeastern US coast, home to the Chesapeake Bay.

The Chesapeake Bay is the largest and one of the most productive estuaries in the continental United States (Bilkovic et al., 2019) (Fig. 1). The Chesapeake Bay has seen a trend of long-term warming (Hinson et al., 2022; Ding & Elmore, 2015), and increasing temperatures have been linked to growing hypoxic conditions in the Bay (Du et al., 2018). In addition to long-term warming, previous work has identified MHWs in the Chesapeake Bay using buoy data (Mazzini & Pianca, 2022; Shunk et al., 2024). Extreme temperatures in 2005 caused an over 50% loss in the seagrass species *Z. marina* in which fisheries species find nursery habitat (Lefcheck et al., 2017). As a result, the area saw declines in three commercially important fish species (Smith et al.,

2023). A report by the Scientific and Technical Advisory Committee, an independent group which provides scientific and technical guidance on environmental issues in the Chesapeake Bay, specifically highlighted the need to develop a marine heatwave warning system due to the impact on living resources (Batiuk et al., 2023).

Here, we use sea surface temperature (SST) satellite data to evaluate the occurrence and characteristics of MHWs in the Chesapeake Bay over a 21-year period, looking at average characteristics as well as long-term trends. We specifically focus on patterns in the characteristics of MHWs including duration, maximum intensity, cumulative intensity, and rates of onset and decline. MHW characteristics are critical for assessing the potential ecological impact and as potential guidance toward understanding the physical causes of MHW. Furthermore, we investigate Chesapeake Bay MHW using observations at a new level of geographic detail, as satellite data enables spatial coverage that is not possible with in situ data alone. Past work using buoys did not find significant differences between the surface expressions of MHW characteristics in the different regions of the Chesapeake Bay

Study Site: The Chesapeake Bay

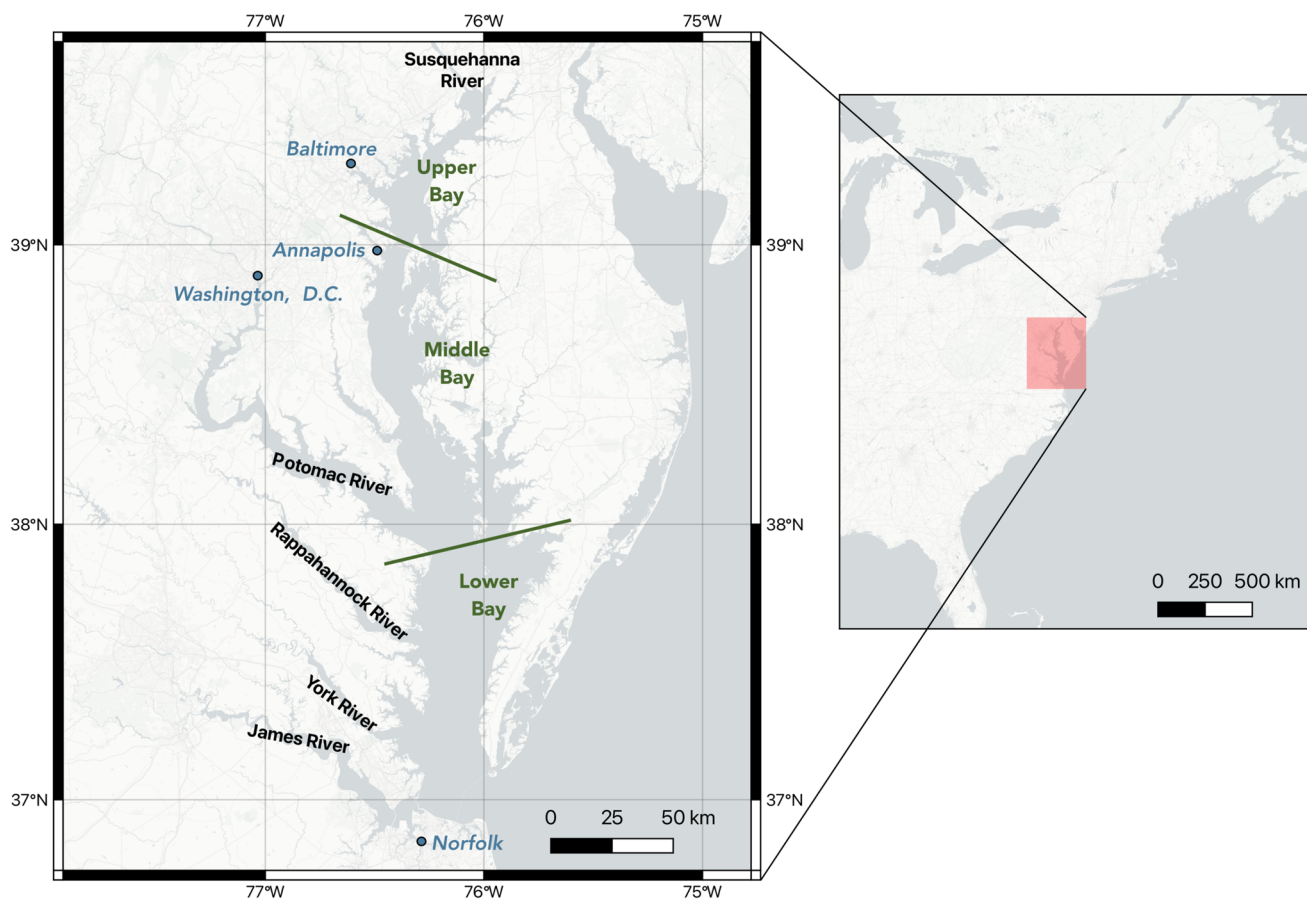


Fig. 1 A map of the Chesapeake Bay, including major rivers referenced throughout this study

(Mazzini & Pianca, 2022); however, we find that there is spatial variation in the surface expression of several defining characteristics of MHWs. Finally, the use of satellite data to investigate MHWs in an estuary setting is novel. Despite the relatively limited horizontal resolution of the observations relative to the size of the Bay, the results and validation presented here suggest this approach can be useful for understanding both temporal and spatial variability of MHWs in estuarine ecosystems such as the Chesapeake Bay.

In the “[Methods](#)” section, we introduce the chosen datasets and describe the definition of MHWs and MHW characteristics. In the “[Results](#)” section, we discuss the validation of the satellite data. We also discuss the spatial and temporal patterns in MHWs characteristics. In the “[Discussion](#)” section, we conclude by summarizing our major findings and propose routes for future analysis.

Methods

Satellite Data Sources

The satellite data products potentially suitable for this study are those with a fine spatial grid, a daily frequency, and a long operating period. The need for the high spatial grid is driven by the size of the Chesapeake Bay. The need for a daily frequency is due to the 5-day length definition for an MHW. Finally, the need for a long operating period is driven by the baseline climatology required for MHW calculations. Hobday et al. (2016) recommends a 30-year climatology. However, past work has shown no appreciable difference in MHW duration or intensity calculated from climatologies based on records as short as 10 years when compared with those calculated using the recommended 30-year time series (Schlegel et al., 2019).

Three satellite SST products fulfilling these criteria were evaluated as candidates for this study: NASA MUR v4.1, NOAA Geo-Polar Blended v2.0, and Copernicus Marine OSTIA v1.3.5. NASA MUR is a daily ~1 km level 4 product based on nighttime SST observations and provides an estimate of the foundation temperature (Chin et al., 2017). Foundation temperature, as defined by the Group for High-Resolution Sea Surface Temperature (GHRSSST), is the temperature at a depth free of diurnal variability (Donlon

et al., 2007). NOAA Geo-Polar is also a daily level 4 product and has ~5 km grid resolution (Maturi et al., 2017). Copernicus Marine OSTIA is a daily level 4 product which also has ~5 km grid resolution (E.U. Copernicus Marine Service Information (CMEMS), 2023; Donlon et al., 2012). These level 4 products provide variables derived from a combination of multiple other measurements (The Group for High Resolution Sea Surface Temperature Science Team et al., 2022). Geo-Polar provides estimates of both daytime and nighttime SST. In this study, nighttime SST is used to more closely estimate the foundation temperature for comparison with NASA MUR and Copernicus Marine OSTIA. See Table 1 for a summary of the three datasets. All datasets are gap-filled such that any no-data values (ex. data gaps caused by clouds) are filled in by spatial and temporal interpolation with estimated SST values. Seven days of data in the Geo-Polar dataset were removed by NOAA data processing due to quality control, as were 3 days of the MUR dataset. These missing days were linearly interpolated in time for each pixel when generating the climatology.

Marine Heatwave Calculation, Characteristics, and Long-Term Trends

Hobday et al. (2016) established the canonical definition of an MHW: an MHW occurs when the temperature rises above the 90th percentile temperature for that day and persists above the daily 90th percentile value for at least 5 days. This is illustrated in Fig. 2a. If an event exceeds the 90th percentile threshold but does not last 5 days it is called a heat spike. The time period for the climatology is the full dataset time period, Jan. 1, 2003, to Dec. 31, 2023 (21 years). Again following Hobday et al. (2016), the 90th percentile threshold for each day uses the days from a centered 11-day window. After the threshold is calculated, the values are smoothed using a 31-day moving average. If multiple MHWs longer than 5 days occur within 2 days of each other they are considered to be a single MHW event. MHWs were calculated using the Python software package marineHeatWaves (Oliver, 2023). The procedures described above are the defaults of this package and are consistent with the recommendations in Hobday et al. (2016).

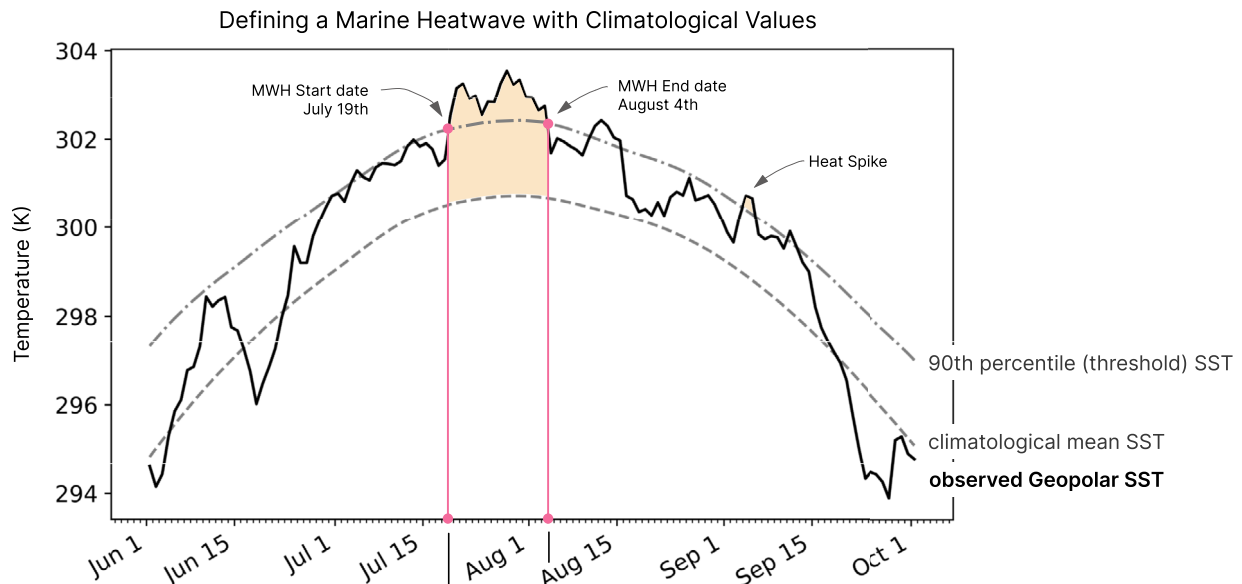
In addition to identifying MHW, the MHW processing computes a variety of MHW characteristics, which allow us

Table 1 Satellite SST data sources

Product name	Version	Organization	Spatial grid	Temporal resolution	Availability
MUR	4.1	NASA	0.01°(~ 1 km)	daily	May 31, 2002 - present
Geo-Polar Blended	2.0	NOAA	0.05°(~ 5 km)	daily	Sept. 1, 2002 - present
OSTIA	3.5	Copernicus Marine	0.05°(~ 5 km)	daily	Dec. 31, 2006 - present

A Marine Heatwave from July 2020

(a)



(b)

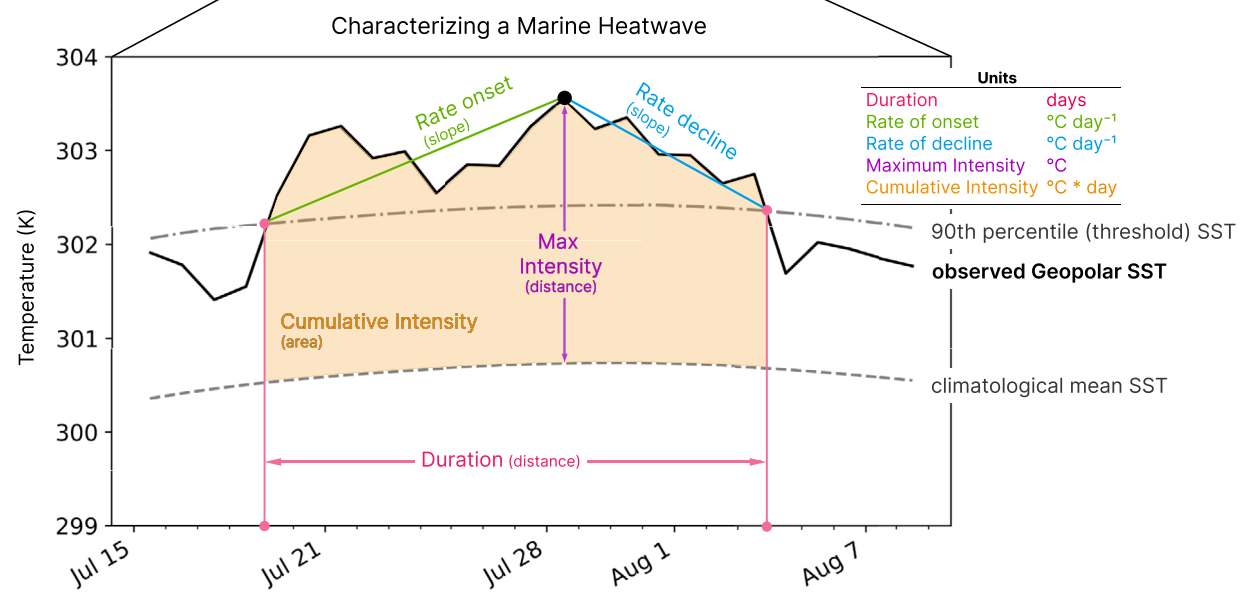


Fig. 2 The observed and climatological values of a MHW from July 2020 in the Tangier Sound in the Middle Chesapeake Bay (38.03°N , 75.97°W), illustrating the definitions of a MHW and MHW characteristics defined in Hobday et al. (2016). **a** visualizes a sustained temperature

anomaly exceeding the 90th percentile threshold value defining an MHW. **b** shows SST focused on the heatwave period, labeling the 5 MHW statistics used in this study to characterize MHWs

to consider different types of MHW. Two extreme temperature events could both be MHW, but still have very different characteristics and thus correspond to different ecological impacts or physical processes of development. The 6 characteristics analyzed in this study are (1) number of annual events, (2) duration, (3) maximum intensity, (4) cumulative intensity, (5) rate of onset, and (6) rate of decline. Figure 2b shows a graphic representation of the MHW characteristics for an example heatwave in July 2020 (see also Hobday et al., 2016).

While most of the analysis presented here used the MHW definition from Hobday et al. (2016), we also performed our analysis using a linearly detrended SST baseline to remove the long-term warming signal. To do this, we performed a linear fit on the raw satellite SST timeseries, then subtracted the linear trend from the SST. After removing the long-term trend the remainder of the MHW calculation was calculated as described in the previous paragraph. These results are discussed in the “[Long-Term Marine Heatwave Trends](#)” section below.

To aid in understanding changes over time an analysis of long-term trends in MHW characteristics is performed. Each pixel in this analysis is treated as an independent time series. Each time series is grouped into annual bins and average MHW characteristics are computed per year. These annual values were then fit to a linear trend and the slope and significance were calculated for the 21-year times series. Significance testing was performed using a one-sided student t-test on each pixel in the bay and spatial patterns were evaluated using multiple hypothesis testing (Wilks, 2016). Multiple hypothesis testing accounts for the number of false positive trends that would be expected in a sample of our size using a false discovery rate, in this study set to 10%.

Satellite Data Validation

In situ data compiled by the Chesapeake Bay Program (CBP) was used to validate satellite SST in the Chesapeake Bay (Chesapeake Bay Program, 2020). The database contains measurements from the CBP partner organizations at long-term, fixed monitoring stations, including ship-based observations. *Traditional Partner Data* from all the programs was used.

The satellite datasets all estimate foundation SST. The in situ data, on the other hand, provide measurements of SST at multiple times of day and depths. To approximate the foundation temperature values from the in situ dataset, only temperature values between 1 and 3 m depth were used. This was done to avoid very near-surface measurements, which are likely subject to stronger diurnal temperature fluctuations. The sensitivity of this depth choice was tested by computing the RMSE between in situ and satellite SST values with several depth choices ranging from 0.5 to 7 m. The RMSE

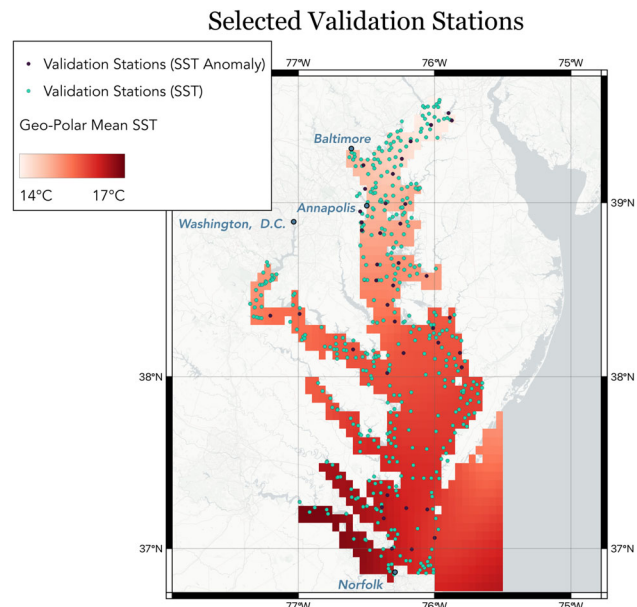


Fig. 3 Locations of CBP validation stations for evaluating the SST (green points) and the SST anomaly (purple points). Underlying imagery is the mean Geo-Polar SST from the study time period of Jan. 1, 2003 to Dec. 31, 2023

changed by 0.1°C or less in all depth choices. The validation period was a 21-year period from Jan. 1, 2003, to Dec. 31, 2023.

Two subsets of the CBP data were used for validation. The first subset is comprised of 483 stations used to validate the SST observations from the satellites. This was done to get an understanding of raw dataset error and may additionally provide insight for other potential uses of satellite SST in the Chesapeake Bay. The second set is comprised of stations with long enough temperature records to generate a climatology and compute the SST anomaly. The analysis from these 51 stations gives an error assessment which is more indicative of expected errors in the MHW calculation. The distributions of each of these two sets of validations are shown in Fig. 3, overlaid on top of the mean SST from Geo-Polar.

To evaluate the accuracy of the three satellite datasets in measuring SST, the observed temperature from each satellite dataset was compared to in situ observations. All satellites have RMSEs of less than 2°C. Geo-Polar had the least mean

Table 2 Satellite SST mean errors

Product name	Slope	Intercept (°C)	RMSE (°C)	R ²	Mean bias (°C)
MUR	0.98	0.15	1.81	0.95	-0.52
Geo-Polar	0.98	0.14	1.57	0.97	-0.50
Blended					
OSTIA	0.97	0.22	1.60	0.96	-0.49

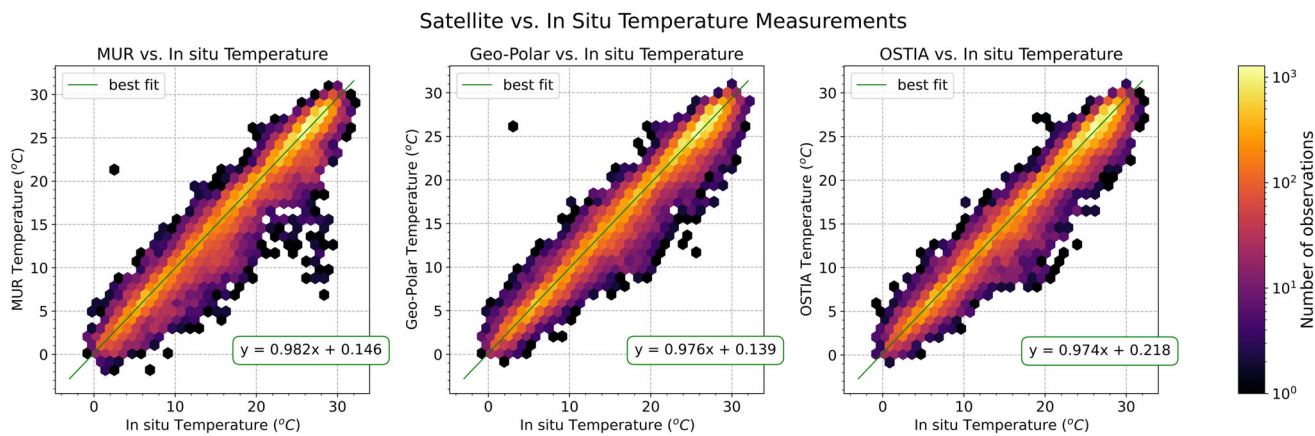


Fig. 4 Density plots of surface temperatures for MUR SST, Geo-Polar SST, and OSTIA SST data products as compared to the Chesapeake Bay Program (CBP) in situ dataset. The left panel shows MUR and the

right panel shows Geo-Polar. Green lines on each plot show the linear fit of observations. Geo-Polar has less variance than MUR, while both datasets underestimate extreme values

error and MUR had the most, although the difference was only about 0.2°C . All datasets are also on average biased about 0.5°C cold. (Table 2). In addition to a smaller RMSE Geo-Polar has less variance than MUR. MUR had more outliers, although all datasets underestimated extreme values (Fig. 4). All datasets are most accurate in the main stem of the Bay and least accurate closer to shore (Fig. 5). Geo-Polar and OSTIA have the largest errors in the upper Potomac and the outflow of the Susquehanna River, while MUR has

the largest errors on the western shore rivers north of Baltimore, such as the Gunpowder and Bush Rivers. MUR also generally has a higher mean error than the Geo-Polar near the Eastern shore. Overall, Geo-Polar and OSTIA are fairly similar. MUR performs on a similar order of magnitude as the other two datasets but is slightly less accurate by most metrics.

Two possible reasons for the land edge cooling effect along the shoreline were considered. These coastal errors could be

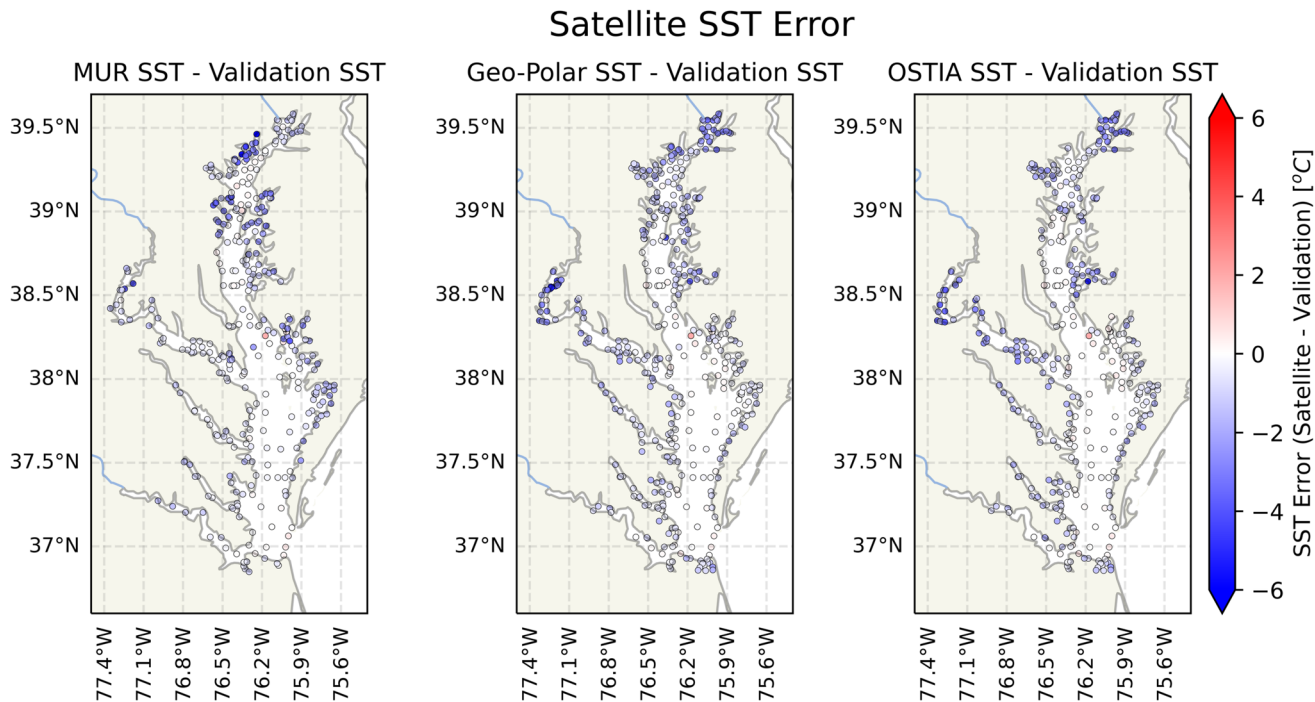


Fig. 5 Spatial distribution of the mean error between the satellite SST datasets and the Chesapeake Bay Program in situ data. Both datasets are most accurate in the main stem of the Bay and have the largest errors near shore. The areas of largest error vary between the two satellites

due to the land surface decreasing temperature faster at night when compared to the ocean, biasing down the observations in nearshore pixels. Another factor may be the different diurnal temperature cycles in the main stem of the Bay and the tributaries. The depth averaging process was done to account for the fact that most CBP measurements were taken during the day. This choice may not mitigate the diurnal cycle of daytime warming in the well-mixed tributaries as well as it does in the deeper, less well-mixed main stem of the Bay.

As extreme temperature events, MHWs are deviations from a climatological mean. Because of this, mean error in the daily climatological SST values does not affect the MHW calculation as it is eliminated when subtracting the daily climatological value from the anomaly SST value. What matters instead is whether the temperature anomaly from the daily climatology (i.e., the difference between the observed SST

and the daily climatological SST value) is accurate. Here, we evaluate the suitability of the satellite SST for analyzing MHWs using the error in the SST anomaly from a daily climatology as opposed to the error in the raw SST value. This method of validation better reflects expected errors in our MHW analysis.

To compare the satellite and in situ data, the SST anomalies were computed for observations over the 21-year period. Due to a sparsity of measurements in the in situ data, the climatologies were computed on a monthly basis. In situ anomaly SST values were then computed as deviations from the monthly climatology. For most similar comparisons of the CBP and satellite datasets a subset of satellite data comprised of days with collocated CBP measurements was used. The same process used for the CBP data was then used for the satellite dataset. A monthly satellite climatological value

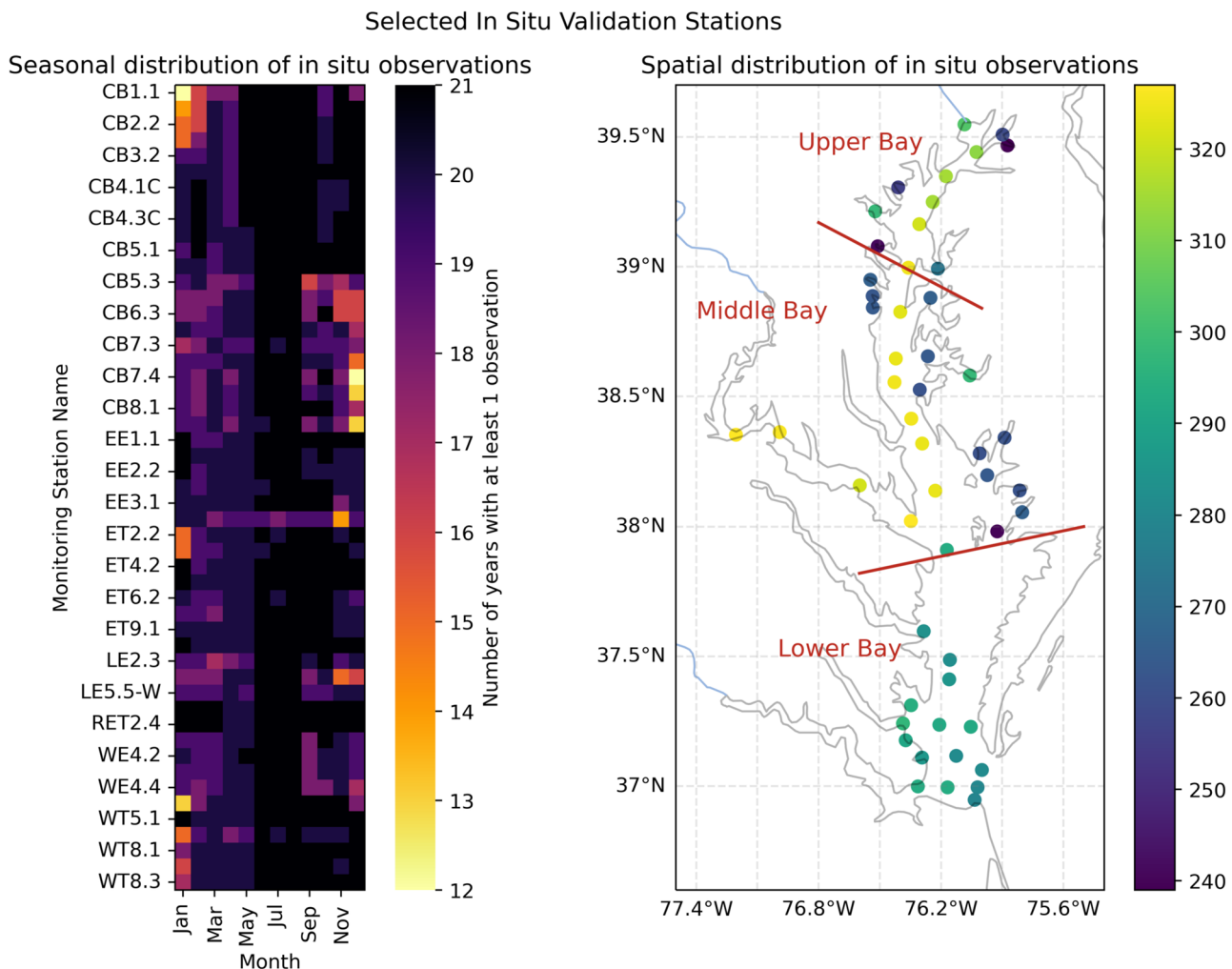


Fig. 6 The left panel shows the monthly distribution of in situ observations for each of the anomaly validation stations used. The color shows the number of months in the 21-year time series that had at least one observation. The right plot shows the spatial distribution of anomaly

validation stations, colored by the total number of observations. Validation stations cover the majority of the main stem of the Bay and several important tributaries. There is a seasonal bias in observations; however, winter months are still represented

Table 3 CBIBS buoy data sources

Buoy name	Section	Approx. latitude	Approx. longitude	Operating years	No. of days of observations
Annapolis	Upper	38.96°N	76.45°W	2013-present	2308
Goose's reef	Middle	38.56°N	76.42°W	2011-present	3107
Stingray point	Lower	37.57°N	76.26°W	2012-present	3532

was computed using the CBP-collocated subset of observations. The anomaly value was computed by subtracting the observed SST from the monthly climatological value. In situ data was compared with the one collocated satellite pixel from the day of the in situ observation. The original in situ dataset was filtered substantially to achieve this calculation. Of the several hundred stations in the CBP dataset, 51 stations were identified with sufficient temporal coverage to compute a climatological baseline. There is a consistent seasonal sampling bias among the CBP in situ stations, in which summers are more highly sampled than winters (Fig. 6). To minimize the impact of this bias on our analysis, stations were vetted by both the number of observations and the monthly consistency of observations. A station needed to have at least one observation every month in at least 57% of the years (12 of 21 years). Stations were also required to have at least one observation per month in 10 of the 12 months in 86% of the years (18 of 21 years). At the end of this station selection process there remained a seasonal sampling bias; however, winter months were still represented.

Figure 6 shows the spatial distribution of the anomaly validation stations. The most important area for our analysis, the main stem of the Bay, is well covered by validation stations, with the exception of one portion of the lower bay. The Potomac River and Susquehanna outflow are also well covered, as are many of the Eastern shore river outflow regions in the upper and middle bay. The major lower Bay rivers, however, including the Rappahannock, the York, and the James, do not have any validation stations with a long enough record to be used for anomaly validation. We, therefore, focus our analysis of tributaries on those with validation stations. Validation data is important for assessing the effectiveness of space-borne satellite monitoring for estuaries such as the Chesapeake Bay. Increased in situ observations (which meet the criteria for evaluating MHWs as described above) in the under-sampled areas of the Bay would be valuable to future investigations.

Finally, we evaluated the likelihood that errors in satellite measurements would correlate temporally causing spurious identification of MHWs. To do this, we computed the temporal autocorrelation of the error in water temperature anomaly from climatology. The in situ dataset does not provide the temporal resolution to compute autocorrelation with a daily lag, so buoy data from NOAA's Chesapeake Bay Interpretive Buoy System (CBIBS) was used instead. Past work comparing buoy data with satellite data can be found in Mazzini and Pianca (2022). We selected 3 buoys, one each in the Upper, Middle, and Lower Bay (Table 3). The Upper Bay buoy only had about 6 years of observations, but was still included for spatial coverage. Only nighttime (12–7 am local time) buoy measurements were used to match the satellite SST foundation temperature definition and missing data in the buoy record was dropped when calculating autocorrelation. The decorrelation timescale was computed and defined as the number of days at which the autocorrelation dropped below e^{-1} .

Effects of Satellite SST Errors on Marine Heatwave Calculations

Using satellite SST in the narrow Chesapeake Bay pushes the limits of these satellite datasets. To understand the potential impact of satellite data on the robustness of the MHW analysis, we considered the following forms of error: (1) mean error, (2) frequency distribution (histogram) of satellite errors, (3) temporal autocorrelation of error, (4) long term and seasonal variability in satellite errors, and (5) spatial variability in satellite errors. Not all forms of errors in the satellite SST product, however, will propagate to the MHW calculation in the same way.

To assess the mean error between the satellite and in situ, SST anomaly estimates of slope and root mean squared error (RMSE) were used (Table 4). Due to the presence of outliers

Table 4 Satellite SST anomaly mean errors

Product name	Slope	Intercept (°C)	RMSE (°C)	R ²	Mean bias (°C)
MUR	0.86	0.19	1.42	0.53	0.0007
Geo-Polar Blended	0.81	0.01	1.00	0.70	0.0024
OSTIA	0.78	-0.04	1.06	0.67	-0.0995

in this dataset regressions were computed using a robust linear regression with a Tukey Biweight norm. Results from the three satellite datasets were quantitatively similar, with Geo-Polar performing the best in RMSE. The slopes of less than 1 with intercepts close to 0 indicate that both datasets underestimate extreme values, suggesting that our results could be an underestimate of extreme events. All three datasets have very low mean biases, with the largest mean bias being -0.1°C in OSTIA. These relationships and the lower variance of Geo-Polar can also be seen in the distributions of Fig. 7. Underestimates in extreme values would result in lower maximum intensities and could also contribute to lower cumulative intensity, rate of onset, and rate of decline. Due to the lower RMSE, we chose to calculate MHW using the Geo-Polar Blended SST product. The remainder of our validation results are therefore only shown for Geo-Polar.

For the purposes of MHWs, errors need to be adjacent in time to produce false MHW. To evaluate this, we estimate the error decorrelation timescale. For all 3 of the tested buoys, the decorrelation timescale was either 3 or 4 days, less than the 5-day minimum length of an MHW. So while the SST mean anomaly errors are non-negligible they decorrelate on a timescale shorter than the threshold for MHW identification.

Lower-frequency temporal variation is another important form of potential bias in satellite errors. A Hovmöller plot shows there is no consistent seasonality in anomaly errors (Fig. 8). Summers, however, do show a long-term trend in

error from March through August. These months underestimate anomaly values prior to 2011 and overestimate anomaly values in 2011 onward. This increasing long-term error could lead to an overestimate in the long-term trend in summertime MHW occurrences and intensity, discussed further in the “Long-Term Marine Heatwave Trends” section. Hovmöller plots for all three satellites are available in the supplemental material.

Spatially, the mean error displayed very little variation (Fig. 9), indicating that spatial variations in MHW, the focus of this paper, are likely not unduly influenced by satellite errors. In contrast, the long-term trend in the error was largest in the upper bay and insignificant in most of the lower bay. Several of the lower bay tributaries, including the Rappahannock, the York, and the James Rivers, did not have any validation stations (Fig. 6). Because of this, we proceed with caution when interpreting results in these tributaries.

We note the primary caveat in our validation analysis is uncertainty in the approximation of foundation temperature from the in situ data for comparison with satellite SST. While the calculation of foundation temperature in the open ocean is well-established, identifying this depth in the dynamic estuarine setting is more difficult. Some shallow areas of the Bay are very well mixed with no depths free of diurnal temperature variability. Additionally, in estuaries tidal advection and diurnal variability from the solar heating cycle can be of the same order of magnitude. This makes a direct compar-

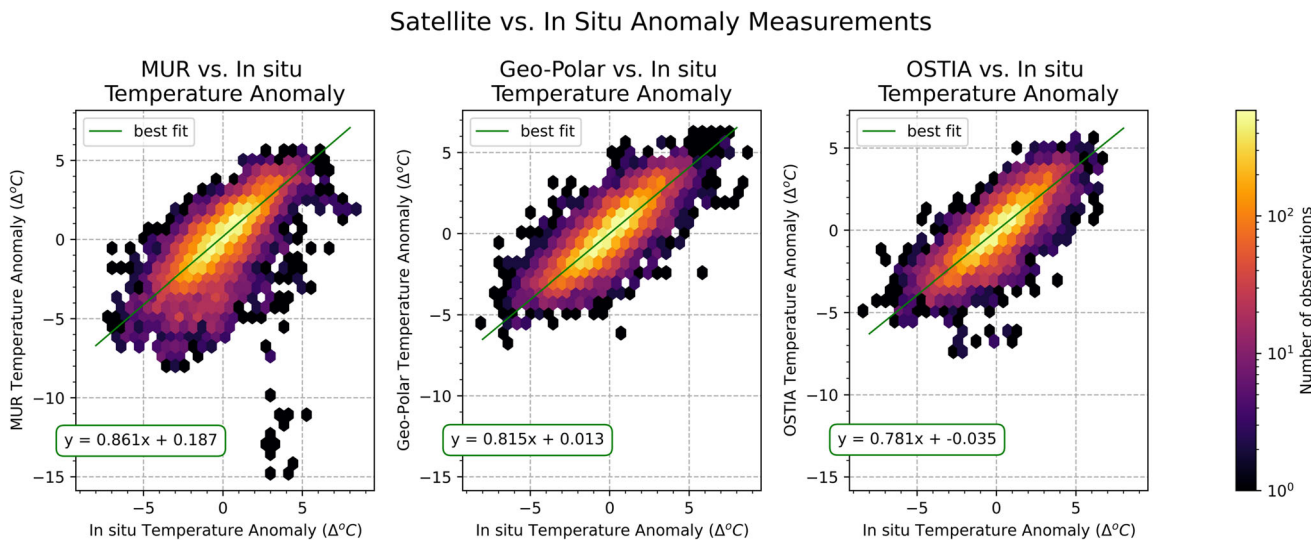


Fig. 7 Density plots of the anomaly error for MUR SST, Geo-Polar SST, and OSTIA SST products as compared to the Chesapeake Bay Program (CBP) in situ dataset. The left, center, and right panels show

MUR, Geo-Polar, and OSTIA, respectively. Green lines on each plot show the linear fit of observations. Geo-Polar has less variance than MUR, while all datasets underestimate extreme values

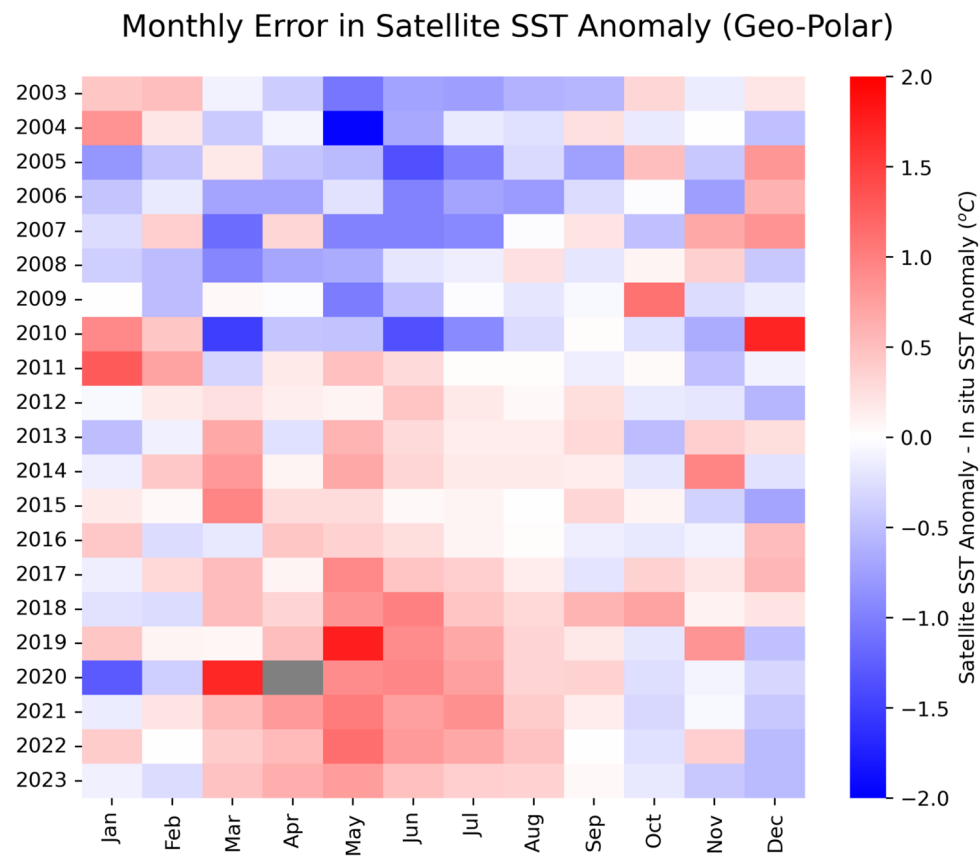


Fig. 8 The error in SST anomalies from climatology for Geo-Polar by month and year. Each pixel corresponds to the average satellite anomaly error for all pixels in the Bay during that year (x axis) and month (y axis). The colorbar shows satellite SST minus in situ measurements, such that

negative (blue) values represent satellite SST underestimates of in situ temperature anomaly. Geo-Polar SST has a long-term trend in the error in SST anomaly from climatology over time in summer months, but no consistent seasonal error

ison between satellite estimates of foundation temperature and in situ SST measurements less clear and complicates error estimation. Overall, we expect our analysis to underestimate the maximum intensity and may overestimate the strength of long-term trends. However, the fast decorrelation timescale of errors relative to the MHW identification threshold is expected to limit the effect of errors on the identified patterns of MHW characteristics. We address the relative magnitudes of these effects in the context of our results in the “Results” section.

Results

Temporal Marine Heatwave Characteristics

Many major documented MHWs in the Northwest Atlantic Ocean also appear in the Chesapeake Bay, including MHWs

in summer 2012 (Mills et al., 2013), winter 2015–2016/fall 2016 (Pershing et al., 2018), and early spring 2017 (Gawarkiewicz 2019). One MHW of particular interest for the Bay was a September 2005 heatwave, during which anomalously high temperatures were shown to decrease commercially relevant seagrass habitat (Smith et al., 2023). The evolution of this MHW is shown in Fig. 10 as an example of the capabilities of the satellite data and to contextualize the aggregate statistics presented later. The MHW first emerged in the center of the Bay, expanded to encompass most of the main stem by the peak, and then receded beginning in the upper Bay. The last area to experience high temperatures was the mouth of the Bay. The strongest anomalies were in the upper bay near Baltimore. While this MHW affected the full Bay and decayed toward the Bay mouth, other MHW shows different patterns of spatial evolution. For example, some MHW begin in the river outflow regions. Additional work could consider these different spatial patterns of evolution and decline, as they may give insight into different driving mechanisms.

SST Anomaly Error and Long Term Change in SST Anomaly Error

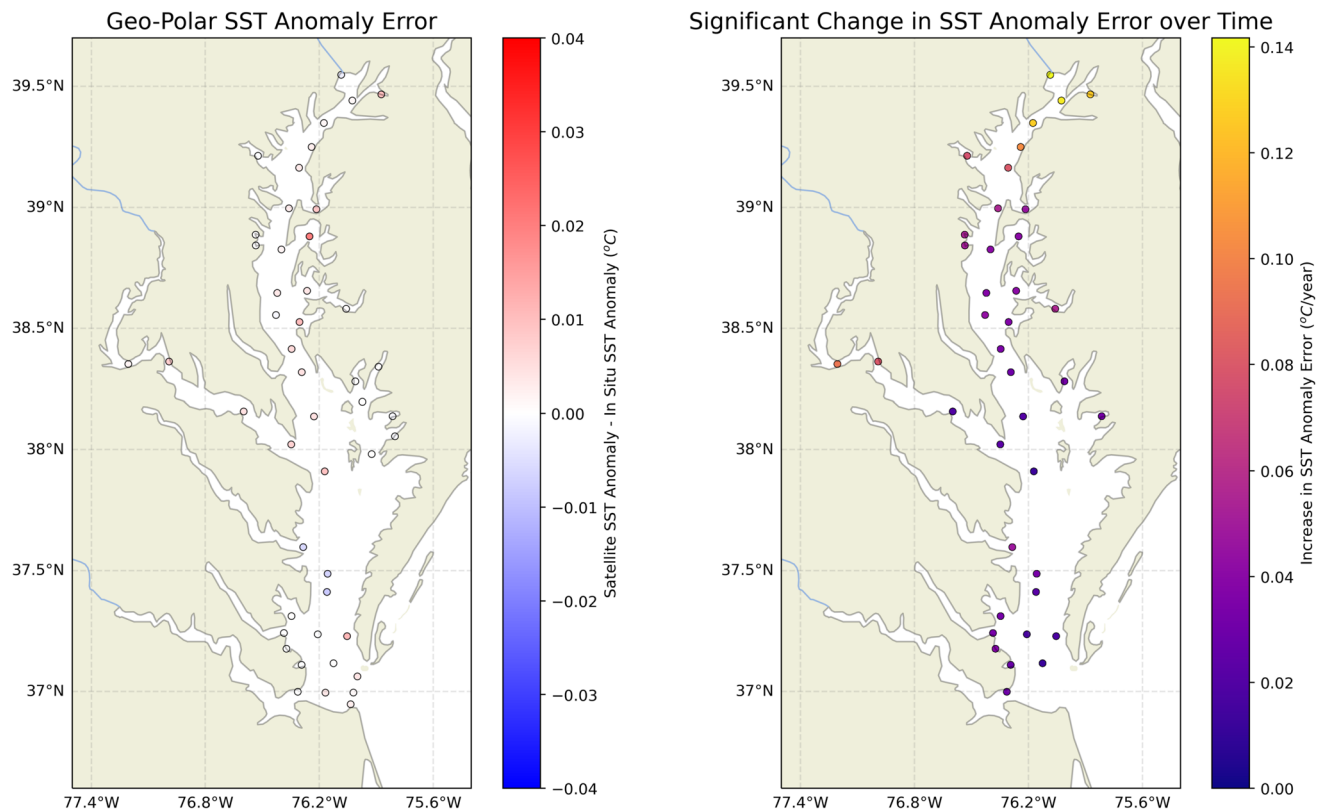


Fig. 9 Maps display the spatial distribution of error across the validation stations. The left figure shows the mean error. The right figure shows the long-term trend in the error. Only stations with a significant trend are displayed (p value less than 0.05). The mean error is

consistent throughout the Bay, but the long-term trend in error shows a north/south gradient, discussed further in the “[Long-Term Marine Heatwave Trends](#)” section

The frequency of MHW in the Chesapeake Bay is increasing over time (Mazzini & Pianca, 2022), consistent with the global trend (Oliver et al., 2018). Figure 11 shows the number of annual MHW events over time in the upper, middle, and lower sections of the Bay. All SST pixels over each of the three sections were averaged together to generate a single annual result. The results from our analysis are shown alongside results from Mazzini and Pianca (2022), which derive MHW frequency from buoy data. There is good agreement between the buoy-derived MHW frequency and the satellite-derived MHW frequency. Mazzini and Pianca (2022) found that there were on average 2 MHW per year with an average duration of 11 days per year, resulting in an average of 22 MHW days per year. The satellite-derived MHW produces consistent results, with a bay-wide average of 2.3 MHW per year and 10.8 days / MHW for a total of 25 MHW days per year. Comparison of these results with Mazzini and Pianca (2022) provides a further form of validation of our approach.

Because MHW is defined relative to a daily climatological baseline, MHW can occur at any time of the year. Figure 12 shows monthly aggregations of MHW for the 6 MHW characteristics. Each MHW in the dataset is counted once and grouped into the month in which it started. Errors in the medians are computing using 2000 iterations of bootstrapping. In the Chesapeake Bay, there is statistically significant seasonality in all six characteristics with an approximate doubling between the minimum and maximum values of each characteristic. MHWs are most prevalent in the Summer with a secondary spike in January. Mazzini and Pianca (2022) also found a summertime peak in MHW; however, because Mazzini and Pianca (2022) aggregate by season instead of month, it is not clear if their buoy-based analysis also showed a January spike. MHW duration has an inverse relationship to the number of MHWs, with duration peaks in March and December. MHW that begin in December and March have durations that are highly variable, as opposed to summer MHW which

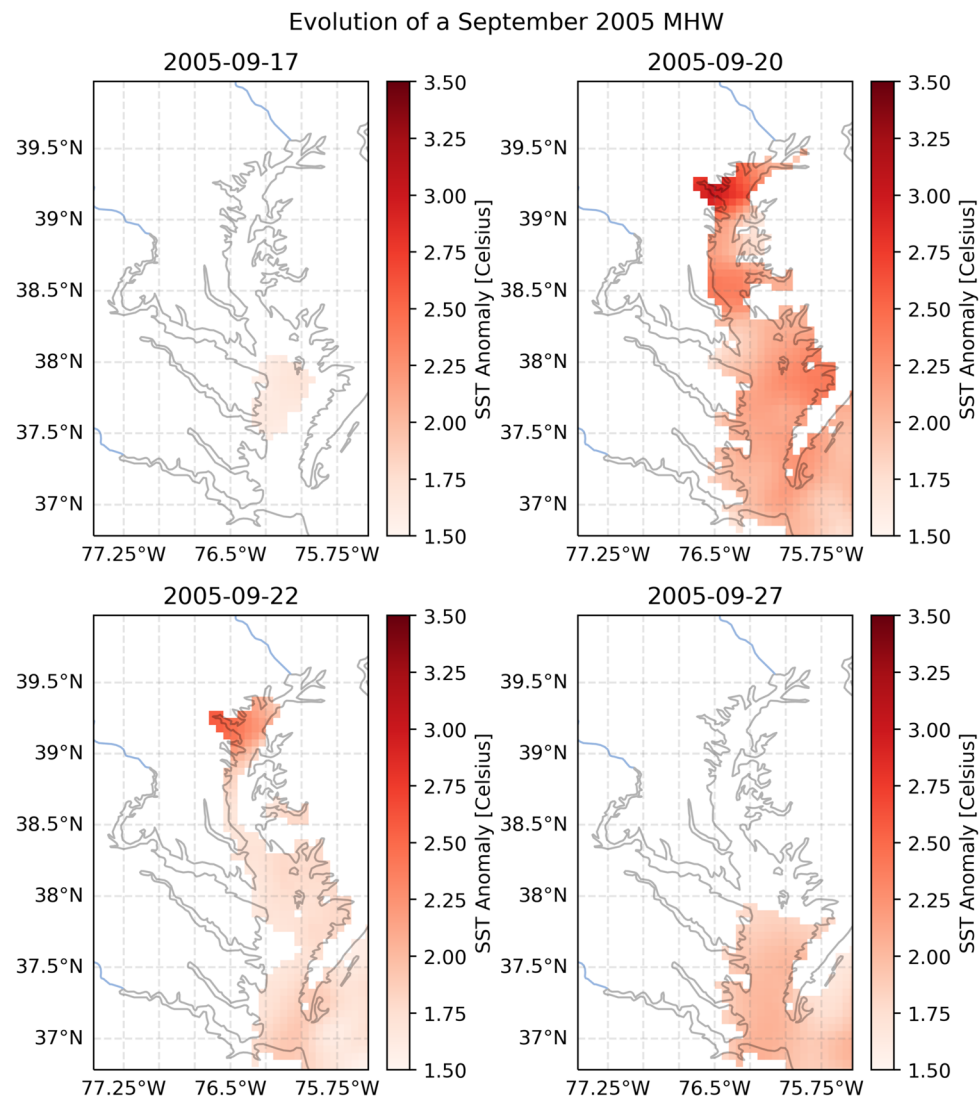


Fig. 10 Evolution of temperature anomaly during a 2005 MHW. The 4 panels show 4 dates throughout the MHW: September 17th, September 20th, September 22nd, and September 27th. Only pixels with an identified MHW are plotted

have more consistent durations. Maximum and cumulative intensity follow the duration pattern, indicating that MHW that begin in March or December are the longest lasting and have high maximum intensities. A subsurface MHW study by Shunk et al. (2024) found that MHW in the Chesapeake Bay follow two regimes: a spring-summer regime where temperature anomalies are confined to the mixed layer and a fall-winter regime that is more vertically homogeneous. The satellite observed seasonality in duration, with the longest MHW in the winter, could be related to the presence of temperature anomalies throughout the water column and slower rates of decline due to the larger volume of water experiencing anomalies. Rates of onset and decline both have peaks in the Spring and Fall, although they differ in that the rate

of onset remains high in January/February while the rate of decline decreases in this same period. The overall variation is large—with all characteristics experiencing at least a doubling between the minimum and maximum months.

The bay-wide average of about 25 MHW days per year is overall spatially uniform (Fig. 13). Considering only MHW days, however, obscures significant spatial variability in the duration and frequency of MHWs in the Bay. An average number of annual MHW and MHW duration show a north-south gradient, ranging from about 2–3 MHW per year and MHW durations between 8 and 13 days. The average number of annual MHW is highest in the northern areas of the Bay while the average MHW duration is highest in the southernmost regions of the Bay. The counteracting north-south

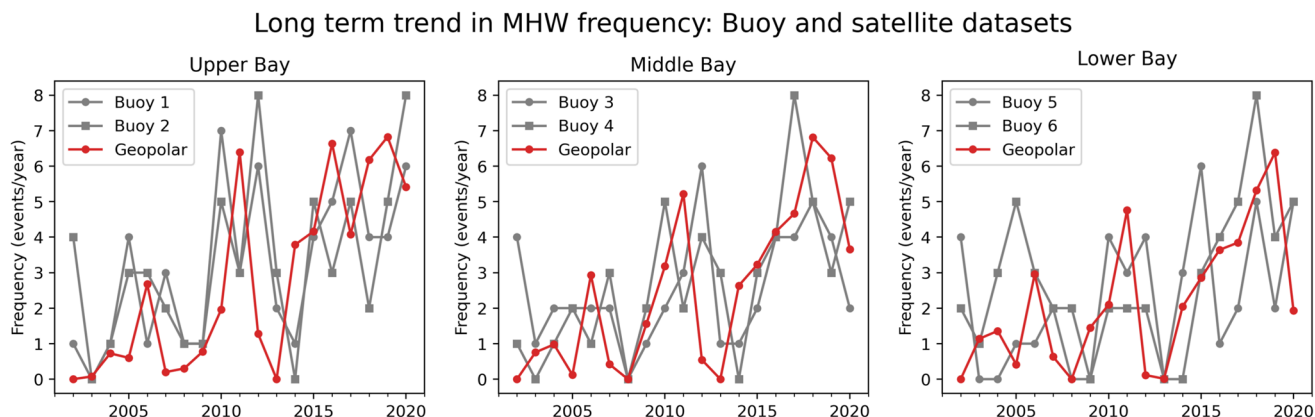


Fig. 11 Time series of MHW frequency in the upper, middle, and lower sections of the Chesapeake Bay. (See Fig. 6 for Bay regions). The frequency of MHW is increasing in all three regions of the Bay. Frequency calculated using Geo-Polar SST, plotted in red, is shown alongside

MHW frequency derived from buoys, plotted in gray. Buoy-derived MHW frequency was reported in Mazzini and Pianca (2022). Regional MHW frequencies are consistent between Geo-Polar and buoy-derived MHW characteristics

gradients of these two fields lead to the uniform pattern of MHW days. To summarize, over the last 21 years in the Chesapeake Bay longer, less frequent heatwaves are found in the southern regions of the Bay while shorter, more frequent MHW characterize the northern regions. Spatial patterns such as this one are not evident when viewing averaged quantities, as the overall number of MHWs days does not vary significantly across the Bay. In the following section, we direct our focus to further consideration of spatial variability in MHW characteristics.

Marine Heatwave Characterization

Satellite observations give a finer-grained look at the development and spatial structure of MHWs. This information can suggest physical mechanisms behind MHW development or decay or provide higher-resolution insights for resource managers. Here, we look at spatial variability in 6 MHW characteristics, each of which indicates something different about the evolution or potential impact of the MHW. The 6 characteristics are (1) average number of annual events, (2) average MHW duration, (3) average maximum intensity, (4) average cumulative intensity, 5 average rate of onset, and (6) average rate of decline. The first two characteristics are shown in Fig. 13, and the remaining 4 characteristics are shown in Fig. 14.

MHW characteristics were aggregated to produce maps showing the average value for each characteristic across the full 21-year time series. The end result is 6 maps, one for each of the aggregated MHW characteristics across the Bay. In addition to the 6 aggregated characteristics in the diagram,

average intensity was considered, but was found to closely follow patterns in the maximum intensity and therefore is not shown here.

The dominant pattern of spatial variation in MHW characteristics is a north-south gradient in the number of events and duration, as discussed in the “[Temporal Marine Heatwave Characteristics](#)” section. This north-south pattern is also evident in cumulative intensity. Cumulative intensity is a reflection of two aspects of a heatwave: duration and intensity. An MHW can have high cumulative intensity either because the MHW has a long duration, it has high maximum intensity or both. In the Chesapeake Bay, MHW cumulative intensity is largest near the mouth of the Bay and minimum in the upper bay, suggesting it is more strongly influenced by duration than by maximum intensity (Fig. 14). Average MHW duration doubles between the lowest and highest values in the Bay, while average maximum intensity changes by only a factor of about 1.3. One deviation from the overall north-south gradient is the estuarine turbidity maximum (ETM), located just north of Baltimore ($\sim 39.3^\circ\text{N}$). The ETM is a region of increased turbidity where salty ocean water collides and mixes with fresh river outflow. The ETM can be seen distinctly in 5 of the 6 MHW characteristics, including in characteristics that do not have a north-south gradient (maximum intensity and rate of decline).

Because maximum intensity is the maximum temperature anomaly relative to the daily climatological baseline, high maximum intensities could be a result of a larger standard deviation in temperature values in a particular section of the Bay. The high maximum intensity could also be related to depth, as the shallower water may heat more effectively during an MHW; however, we did not find depth to be strongly

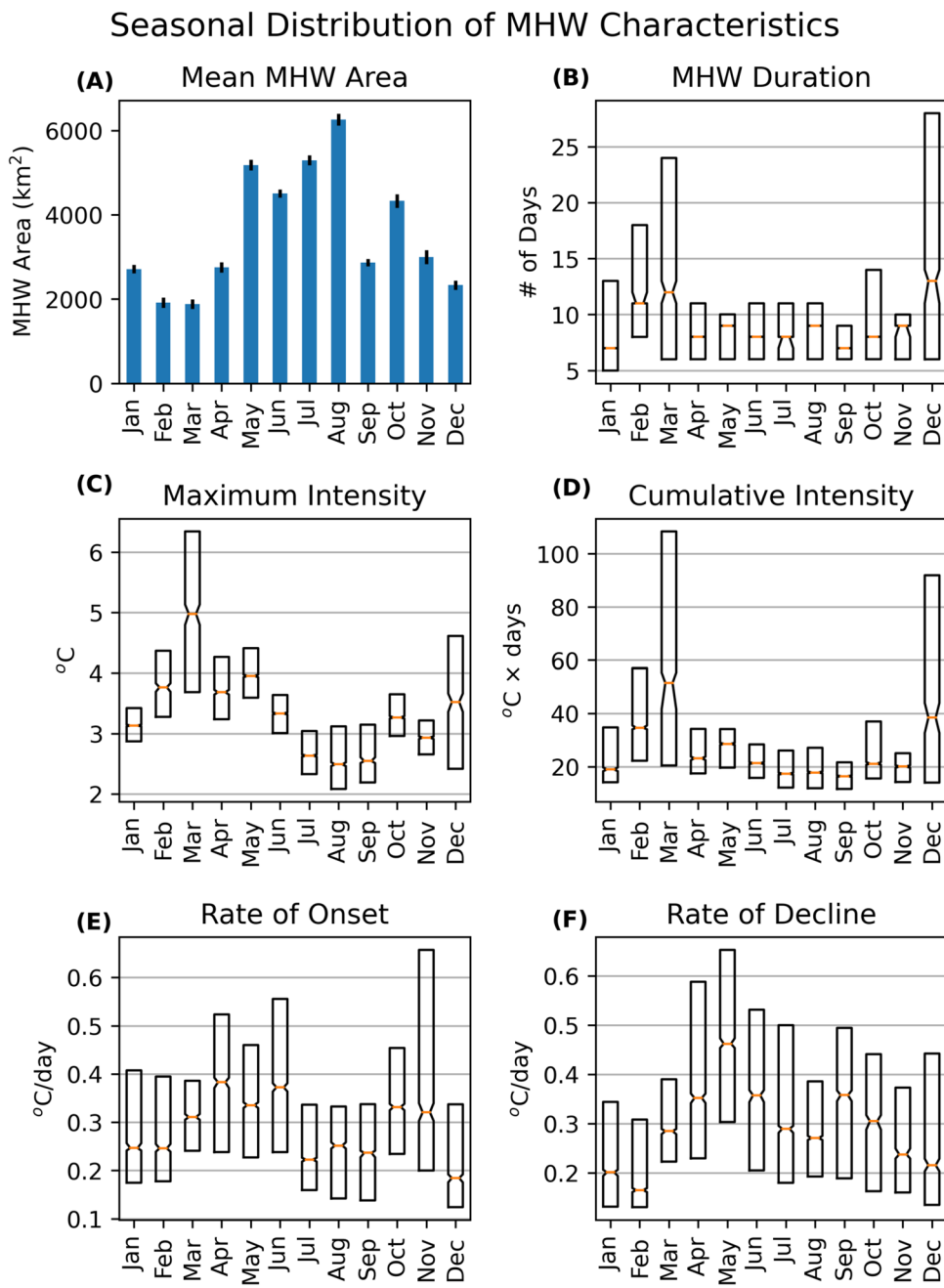


Fig. 12 Monthly distributions of six MHW characteristics defined as shown in Fig. 2: **A** the mean area experiencing an MHW with error bars, **B** MHW duration, **C** maximum intensity, **D** cumulative intensity, **E** rate of onset, and **F** rate of decline. **B–F** each show the 25th, 50th, and 75th percentile values in the box plots. The error, computed using 2000

iterations of bootstrapping, is represented by a notch in the box plot. The error bars in **A** are computed using the standard error of the mean. Each MHW is counted in the month in which it started. There is clear seasonality in all of the characteristics, with an approximate doubling between maximum and minimum monthly values

correlated to MHW intensity (see supplemental material). Past work has shown that low-land rivers are extremely sensitive to air temperature (Piccolroaz et al., 2018), a common driver of marine heatwaves.

The rate of onset and decline are two particularly important characteristics for understanding the mechanisms of

MHW development and decline. The rate of onset showed an approximately 1.5-fold difference between the highest and lowest values in the Bay (Fig. 14). MHW develops the quickest in the upper Bay where temperature anomalies can increase at almost 0.5°C per day. Relative to the rate of onset, the rate of decline is more uniform in the main stem of the

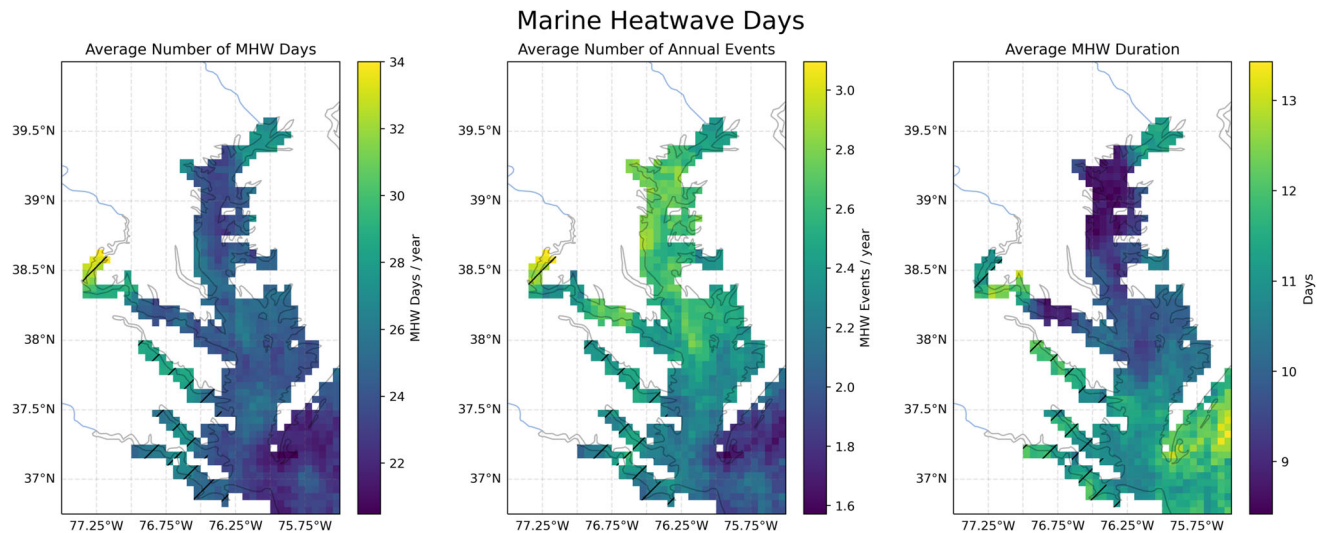


Fig. 13 The spatial distribution of the average number of MHW days per year using Geo-Polar SST. The average number of MHW days is calculated by multiplying the average number per year by the average duration. Hashed lines denote areas where anomaly SST validation data is not available

bay (approximately 0.4°C/day). Shunk et al. (2024) found that air-estuary heat flux changes, primarily from latent heat, are the leading driver of MHW onset and decline in the Chesapeake. However, the spatial variability in rates of onset and decline in the satellite data may suggest an additional role for other processes in the development and decay of MHW in the main stem of the Bay. Further investigation into the finer-scale spatial structure of the rates of onset and decline could be an avenue of future research into drivers of MHW in the Bay.

Long-Term Marine Heatwave Trends

Our analysis of long-term trends (see the “[Marine Heatwave Calculation, Characteristics, and Long-Term Trends](#)” section) suggests that almost the entire Bay is experiencing significant increases in the number of annual MHW events (Fig. 15). The largest values are close to an increase of about 5 additional MHW events per decade, or an approximately 10% increase in number of annual MHW events over the period of 2003–2023. There is significant spatial variation, seen in the factor of 3 difference between the highest and lowest rates of increase in annual MHW events. The upper Bay, which experiences the most frequent but shortest MHW, is also the area that has the greatest increases in the number of MHW. The only section of the Bay that does not see significant increases in the number of events is the mouth of the Bay. In contrast, average duration and cumulative intensity did not show statistically significant increases over this time period. Given that cumulative intensity structure was controlled by

duration we would expect that these two would show a similar trend, or lack thereof. In summary, we are seeing that for most of the main stem of the Bay, the qualitative character of MHWs is not changing, as MHWs are not longer nor are they more intense, but there are more MHWs occurring. This extends the findings of Mazzini and Pianca (2022), who found increases in frequency but no trend in duration at several moorings in the Bay over their study period, 1986–2020.

The error analysis in the “[Effects of Satellite SST Errors on Marine Heatwave Calculations](#)” section revealed spatial variability in the long-term error that mirrored the observed trend for a number of MHW: largest in the upper Bay and decreasing to the south. While this trend could raise concerns about the observed spatial patterns, the relative magnitudes of the error and the observed signal give confidence in the results. In the upper Bay, the error in long-term trend is the largest, at $\sim 1^{\circ}\text{C}/\text{decade}$ (Fig. 9). The observed increase in MHW intensity upper Bay shows an increase of about 2.4°C per decade (upper right panel of Fig. 15). Subtracting the calculated error from the MHW intensity implies there is still, at a minimum, 1.4°C per decade increase in MHW intensity in this portion of the Bay.

While a large body of MHW literature has centered on the definition of an MHW with a fixed climatological baseline described in Hobday et al. (2016), there is a growing body of work utilizing a detrended SST for the climatological baseline (ex. Jacox et al., 2020). These two approaches provide different insights into future change and resource management (Amaya et al., 2023). Here, we calculate an annual number of MHW events with a detrended SST to highlight which aspects of the spatial pattern are related to long-term

MHW Characteristic Maps

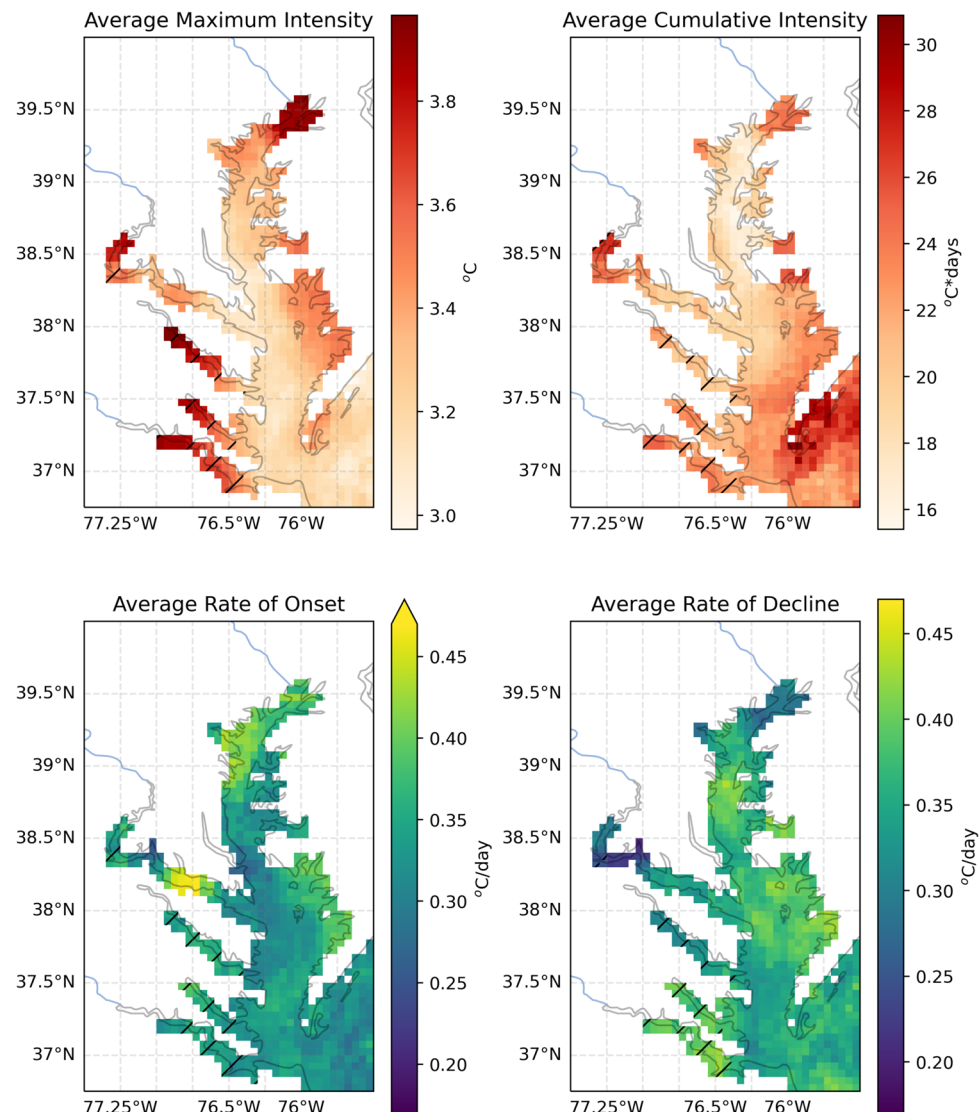


Fig. 14 Spatial maps showing the distribution of 4 MHW characteristics. Maps show an aggregation (either sum or average) of across time for each pixel. Hashed lines denote areas where anomaly SST validation data is not available

warming as opposed to changes in extreme events. The differences between the fixed and detrended climatologies suggest that the processes that generate MHW in these locations are attributable to long-term warming. This is the case for much of the upper Bay and is shown in red in Fig. 16C. This decrease in MHW events in the upper Bay is also seen in the weaker north/south gradient in the detrended MHW analysis.

These data suggest that changes in MHW in the Chesapeake are not due to changes in the spread of temperatures, or an increase in extreme values, but rather due to changes in the mean temperature. There are no significant long-term trends in any MHW characteristic when computing MHW characteristics using the detrended climatology, evidence that

increases are due to changes in the mean temperature. Past work has also attributed MHW trends to a long-term change instead of increases in extreme temperature values (Mazzini & Pianca, 2022).

Discussion

Estuarine environments provide critical ecological and economic value; however, studies of estuarine marine heatwaves have been scarce. Availability of monitoring data is a common limitation, and buoy data does not provide a highly

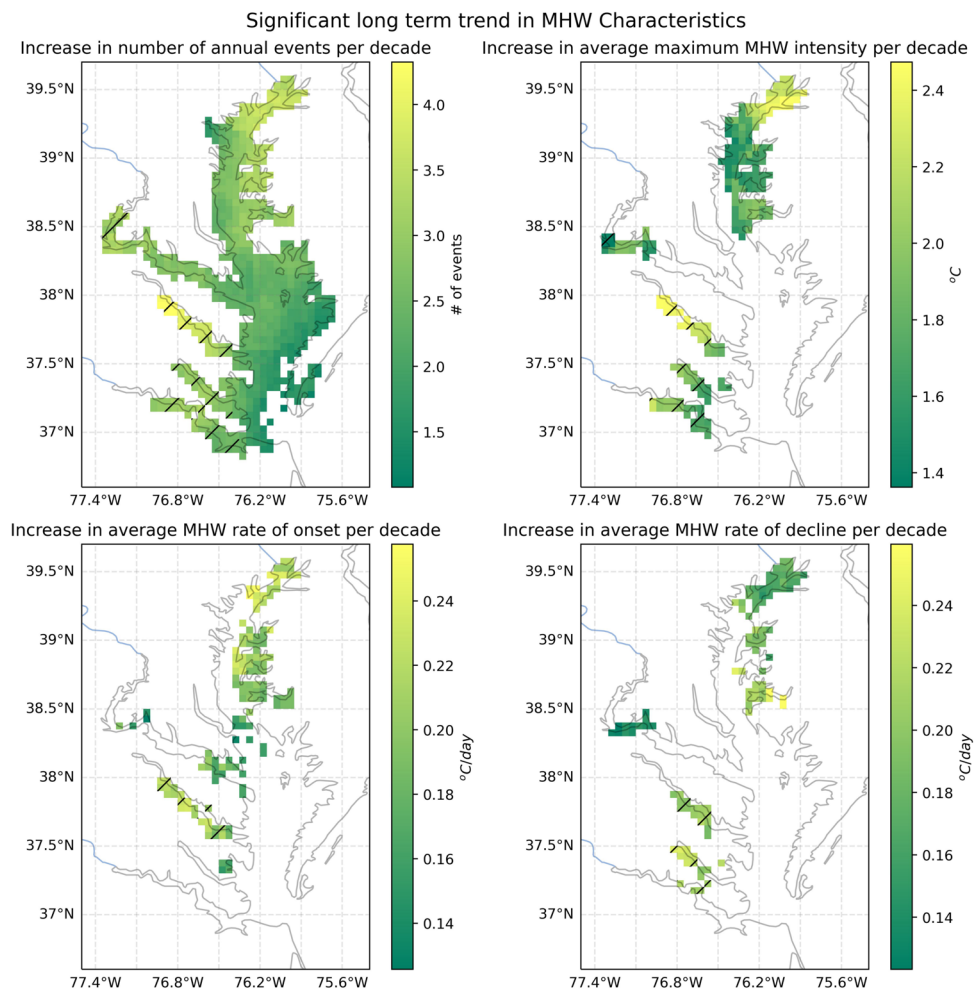


Fig. 15 Long-term trends in MHW characteristics. Plots show the slope of a linear regression on each pixel in increases per decade. Only those pixels considered statistically significant under multiple hypothesis test-

ing with a false discovery rate of 10% were included. Hashed lines denote areas where anomaly SST validation data is not available

resolved spatial structure, which can limit understanding of impacts and drivers. Here, we used satellite data to provide a novel, spatially resolved picture of MHW in the Chesapeake Bay.

Three satellite SST sources, NASA MUR, NOAA GeoPolar, and Copernicus Marine OSTIA, were evaluated against in situ measurements. All datasets likely underestimate extreme values and over estimate summertime long-term trends but show spatial consistency in SST anomalies. Validation work such as this is critical for the accurate interpretation of global SST datasets in coastal zones. This validation was possible because of the availability of in situ validation data, but this resource is not as widely available in every estuary. While estuaries differ in dynamic conditions and seasonal variability, the successful use of satellite SST in the Chesapeake suggests that the application of satellite SST for spatially resolved temperature studies in other large estuaries may be possible. The use of well-calibrated

regional models may provide an alternate method for validating the use of satellite data in estuaries where there is otherwise insufficient in situ data.

MHW characteristic maps reveal spatial variation in the Chesapeake, where the dominant pattern of variability is a north-to-south (along estuary) gradient. The spatial structure reveals that cumulative intensity is dominated by MHW duration, not max intensity. This result, coupled with the strong bay-wide variation in MHW duration, highlights MHW duration as a key MHW characteristic in the Chesapeake Bay. Temporal MHW analyses show increases in MHW frequency over time and an average of 25 MHW days per year bay-wide. Increases in MHW events in the lower Bay result in approximately 5 additional annual events per decade, a near doubling of MHW frequency over the 21-year satellite period. Comparison of these results with a detrended SST analysis suggests that long-term warming influence on MHW characteristics is particularly influential in zones of

Number of MHW Events under Shifting vs. Fixed Climatology

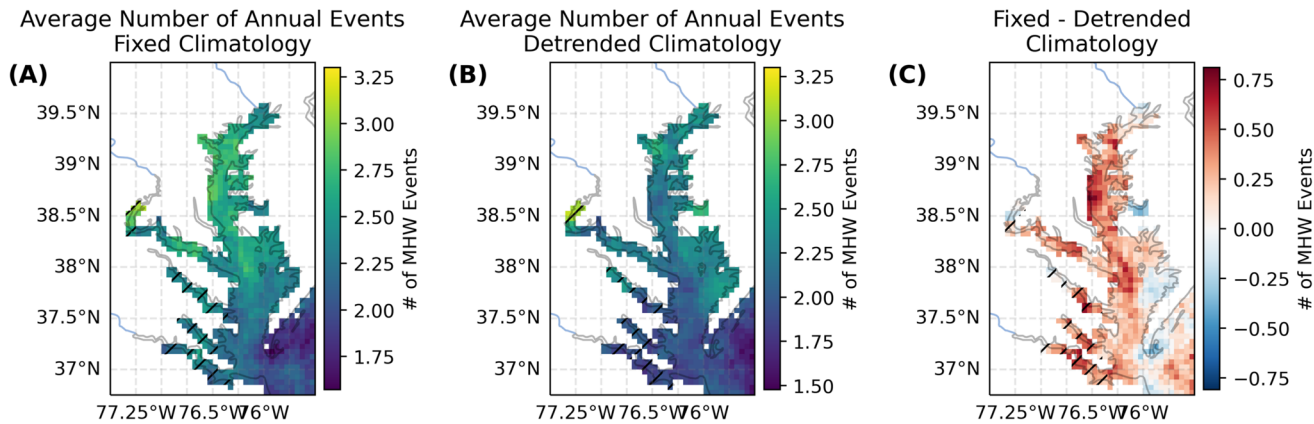


Fig. 16 Aggregated maps showing the average number of annual MHW events using **A** unmodified SST and **B** detrended SST. **C** The difference of the two. Red zones in **C** show where MHWs are attributable to long-

term warming. We see the strong influence of long-term warming on the number of annual MHW events in the upper Chesapeake Bay. Hashed lines denote areas where anomaly SST validation data is not available

river influence. Confidence in long-term trends is tempered by changes in satellite error over time, pointing to the criticality of periodic reanalyses of satellite data to identify and correct for systematic errors. Satellite-derived MHW analysis is consistent with past buoy-based analysis from Mazzini and Pianca (2022), giving confidence in the accuracy of this new technique. Given that the satellite data likely represents an underestimate of temperature (“[Effects of Satellite SST Errors on Marine Heatwave Calculations](#)” section), it is possible these trends are even stronger. Increased spatial resolution and clarity into regional trends in MHW characteristics benefit our understanding of extreme temperature events in the Chesapeake Bay and could benefit monitoring efforts that help mitigate the high economic impact and conserve protected waters.

The success of this satellite technique for analyzing MHW in rivers is not entirely clear. There are some available validation stations in the Potomac and Susquehanna outflow region; however, the performance of the satellite data in these regions appears mixed. The anomaly SST errors—most relevant for MHW calculations—are relatively small (Fig. 9); however, the large mean SST errors of 3–4° Celsius suggest caution is warranted. In the lower tributaries of the Bay (the Rappahannock, York, or James rivers), we are limited by a lack of long-term monitoring stations in the river tributaries to provide validation data. The relatively small anomaly errors in the Potomac, however, suggest that the satellite data produces reasonable marine heatwave results in the tributaries. The lack of in situ data for observing marine heatwaves highlights the importance of satellite data to provide observational coverage in these regions. The Bay tributary regions are critical areas for resource managers. Further improvement or

algorithmic development focusing on these regions or additional satellite products with higher spatial resolutions would be of scientific and public benefit.

While our results show that increasing MHW is due to long-term warming; past work investigating long-term warming in the Chesapeake Bay shows that surface warming is overall spatially consistent, with only slightly faster warming at the mouth of the Bay (Hinson et al., 2022). The spatial variability seen in this work implies that, while the largest contribution to MHW increase may be long-term warming, there are still additional characteristics, or causes, of MHW that may be changing over time. A more detailed investigation into the dynamical drivers of MHW will be needed to identify why there is a lack of spatial variability in long-term warming but spatial variability in MHW frequency increases.

Global MHW work has found that large-scale atmospheric pressure anomalies are a driver for MHW in the mid and high latitudes (Holbrook et al., 2019). Tassone et al. (2022) looked at estuarine MHW in particular, finding that in the Chesapeake Bay atmospheric and oceanic MHW were co-occurring over 50% of the time, the second highest co-occurrence of the 12 estuaries studied across the United States. The Chesapeake Bay, however, had only the sixth most number of events, highlighting the variability of MHW behavior between estuarine environments. These findings agree with those of Shunk et al. (2024), which found changes in air-estuary heat flux to be the primary driver of MHW onset and decline. While atmospheric MHWs likely have a strong influence in generating MHW in the Chesapeake Bay, Tassone et al. (2022) also found that oceanic MHW tended to lag atmospheric MHW in the Chesapeake Bay by only 1 day, and highlighted that in some cases a relatively low intensity,

low duration atmospheric MHW is enough to push an estuarine environment into an MHW when water temperatures are already elevated.

Future analysis could focus on connecting spatial patterns of MHW characteristics identified here to MHW mechanisms of development and decline in the Chesapeake. Patterns of evolution, such as the example in Fig. 10, hint at multiple spatial patterns of evolution that could indicate differing influences. For example, some MHW appeared to develop starting in the river tributaries and expand to the main stem, while others appeared to begin at the mouth of the Bay, perhaps reflecting the relative influence of rivers and the coastal ocean. Another avenue could be to pursue the spatial patterns in rates of onset and decline. Past work in the North Atlantic suggests that atmospheric mechanisms are the most influential mechanism in MHW development while ocean processes are the more influential mechanism in MHW decline (Schlegel et al., 2021). The rate of onset and decline in the Chesapeake Bay showed the finest scale spatial structure of the metrics considered here, and differences in their distributions could be related to mechanistic influence.

The Chesapeake Bay is the largest estuary in the continental US and the impacts of a warming climate have societal and economic impacts. This work provides a spatial analysis of MHW characteristics and trends in the Chesapeake. Validation of satellite SST in the Bay allows future researchers to more accurately understand results derived using SST in the Bay. Spatial variation in MHW characteristics highlights the importance of spatial structure in the Bay, highlights the differences between river regions and main stem waters, and provides initial insight into possible MHW mechanisms.

Supplementary Information The online version contains supplementary material available at <https://doi.org/10.1007/s12237-025-01546-9>.

Acknowledgements The authors would like to acknowledge that this work would not have been possible without the contributions of many open source software libraries, including pandas (pandas development team, 2020), xarray (Hoyer & Hamman, 2017), project jupyter (Kluyver et al., 2016), scipy (Virtanen et al., 2020), dask (Dask Development Team, 2016), matplotlib (Hunter, 2007) and cartopy (Met Office, 2010 - 2015).

The scientific results and conclusions, as well as any views or opinions expressed herein, are those of the author(s) and do not necessarily reflect the views of NOAA or the Department of Commerce.

Author Contribution Rachel Wegener: conceptualization, methodology, software, investigation, data curation, writing—original draft, visualization. Jacob Wenegrat: conceptualization, methodology, writing—review and editing, supervision, project administration. Veronica P. Lance: conceptualization, methodology, writing—review and editing, supervision, funding acquisition. Skylar Lama: software, formal analysis, data curation.

Funding This study was supported by NOAA grant NA19NES4320002 (Cooperative Institute for Satellite Earth System Studies-CISESS) at the

University of Maryland/ESSIC. Jacob Wenegrat acknowledges support from NSF award 2126474.

Data Availability Processed data used to generate all figures is available in the Sea Scientific Open Data Edition (SEANOE) (DOI: 10.17882/105013). This includes:

1. SST values for Chesapeake Bay Program data and each of the satellite datasets at each of the dates and locations used (csv file format). Used to generate Figs. 4 and 5.

2. SST anomaly values for Chesapeake Bay Program data and each of the satellite datasets at each of the dates and locations used (csv file format). Used to generate Figs. 7, 8, and 9.

3. Average MHW characteristics for each pixel based on Geo-Polar SST (netcdf file format). Used to generate Figs. 13, 14, 15, and 16.

Raw SST data from NOAA Geo-Polar, NASA MUR, Copernicus Marine OSTIA, and the Chesapeake Data Program has also been submitted to SEANOE for ease of replication. Satellite datasets (Geo-Polar, MUR, and OSTIA) which have been subset to the Chesapeake Bay region and study time frame are available in the netcdf file format. Geo-Polar SST was used to generate Fig. 10. Chesapeake Bay Program in situ water temperature measurements subset to the Chesapeake Bay and study time frame are also available in the SEANOE repository (csv format).

Code Availability The code associated with the article can be accessed via Github (https://github.com/rwegener2/journalarticle_chesapeake_mhw). An archive copy is also available on Zenodo (DOI: 10.5281/zenodo.15243231).

Declarations

Competing Interests The authors declare no competing interests.

Open Access This article is licensed under a Creative Commons Attribution 4.0 International License, which permits use, sharing, adaptation, distribution and reproduction in any medium or format, as long as you give appropriate credit to the original author(s) and the source, provide a link to the Creative Commons licence, and indicate if changes were made. The images or other third party material in this article are included in the article's Creative Commons licence, unless indicated otherwise in a credit line to the material. If material is not included in the article's Creative Commons licence and your intended use is not permitted by statutory regulation or exceeds the permitted use, you will need to obtain permission directly from the copyright holder. To view a copy of this licence, visit <http://creativecommons.org/licenses/by/4.0/>.

References

- Amaya, D. J., Jacox, M. G., Fewings, M. R., et al. (2023). Marine heatwaves need clear definitions so coastal communities can adapt. *Nature*, 616(7955), 29–32. <https://doi.org/10.1038/d41586-023-00924-2>
- Batiuk, R., Brownson, K., Dennison, W., et al. (2023). Rising watershed and bay water temperatures: Ecological implications and management responses – A STAC workshop. STAC Publication Number 23-001. https://www.chesapeake.org/stac/wp-content/uploads/2023/01/FINAL_STAC-Report-Rising-Temps_April.pdf
- Bilkovic, D. M., Mitchell, M. M., Havens, K. J., et al. (2019). Chapter 15 - Chesapeake Bay. In Sheppard, C. (ed.) *World seas: An environmental evaluation* (Second Edition). Academic Press, pp. 379–404. <https://doi.org/10.1016/B978-0-12-805068-2.00019-X>

- Chatterjee, A., Anil, G., & Shenoy, L. R. (2022). Marine heatwaves in the Arabian sea. *Ocean Science*, 18(3), 639–657. <https://doi.org/10.5194/os-18-639-2022>
- Chesapeake Bay Program (2020). Water quality datahub. <https://datahub.chesapeakebay.net/WaterQuality>
- Chin, T. M., Vazquez-Cuervo, J., & Armstrong, E. M. (2017). A multi-scale high-resolution analysis of global sea surface temperature. *Remote Sensing of Environment*, 200, 154–169. <https://doi.org/10.1016/j.rse.2017.07.029>
- E.U. Copernicus Marine Service Information (CMEMS) (2023). Global ocean OSTIA sea surface temperature and sea ice analysis. <https://doi.org/10.48670/moi-00165>
- Dask Development Team (2016). Dask: Library for dynamic task scheduling. <http://dask.pydata.org>
- Ding, H., & Elmore, A. J. (2015). Spatio-temporal patterns in water surface temperature from landsat time series data in the Chesapeake Bay, U.S.A. *Remote Sensing of Environment*, 168, 335–348. <https://doi.org/10.1016/j.rse.2015.07.009>
- Donlon, C. J., Martin, M., Stark, J., et al. (2012). The operational sea surface temperature and sea ice analysis (ostia) system. *Remote Sensing of Environment*, 116, 140–158. <https://doi.org/10.1016/j.rse.2010.10.017>. Advanced Along Track Scanning Radiometer(AATSR) Special Issue
- Donlon, C., Robinson, I., Casey, K. S., et al. (2007). The global ocean data assimilation experiment high-resolution sea surface temperature pilot project. *Bulletin of the American Meteorological Society*, 88(8), 1197–1214. <https://doi.org/10.1175/BAMS-88-8-1197>
- Du, J., Shen, J., Park, K., et al. (2018). Worsened physical condition due to climate change contributes to the increasing hypoxia in Chesapeake Bay. *Science of The Total Environment*, 630, 707–717. <https://doi.org/10.1016/j.scitotenv.2018.02.265>
- Gawarkiewicz, G., Chen, K., Forsyth, J., et al. (2019). Characteristics of an advective marine heatwave in the middle Atlantic bight in early 2017. *Frontiers in Marine Science*, 6. <https://doi.org/10.3389/fmars.2019.00712>
- Hinson, K. E., Friedrichs, M. A., St-Laurent, P., et al. (2022). Extent and causes of Chesapeake Bay warming. *JAWRA Journal of the American Water Resources Association*, 58(6), 805–825. <https://doi.org/10.1111/1752-1688.12916>
- Hobday, A. J., Alexander, L. V., Perkins, S. E., et al. (2016). A hierarchical approach to defining marine heatwaves. *Progress in Oceanography*, 141, 227–238. <https://doi.org/10.1016/j.pocean.2015.12.014>
- Holbrook, N. J., Scannell, H. A., Sen Gupta, A., et al. (2019). A global assessment of marine heatwaves and their drivers. *Nature Communications*, 10, 2624. <https://doi.org/10.1038/s41467-019-10206-z>
- Hoyer, S., & Hamman, J. (2017). xarray: N-D labeled arrays and datasets in Python. *Journal of Open Research Software*, 5(1). <https://doi.org/10.5334/jors.148>
- Huang, Z., Feng, M., Beggs, H., et al. (2021). High-resolution marine heatwave mapping in Australasian waters using Himawari-8 SST and SSTAARS data. *Remote Sensing of Environment*, 267, 112742. <https://doi.org/10.1016/j.rse.2021.112742>
- Hunter, J. D. (2007). Matplotlib: A 2d graphics environment. *Computing in Science & Engineering*, 9(3), 90–95. <https://doi.org/10.1109/MCSE.2007.55>
- Jacox, M. G., Alexander, M. A., Bograd, S. J., et al. (2020). Thermal displacement by marine heatwaves. *Nature*, 584(7819), 82–86. <https://doi.org/10.1038/s41586-020-2534-z>
- Kluyver, T., Ragan-Kelley, B., Pérez, F., et al. (2016). Jupyter notebooks - A publishing format for reproducible computational workflows. In Loizides, F., & Schmidt, B. (eds.) *Positioning and power in academic publishing: Players, agents and agendas* (pp. 87–90). Netherlands: IOS Press. <https://eprints.soton.ac.uk/403913/>
- Lefcheck, J. S., Wilcox, D. J., Murphy, R. R., et al. (2017). Multiple stressors threaten the imperiled coastal foundation species eelgrass (Zostera Marina) in Chesapeake Bay, USA. *Global Change Biology*, 23(9), 3474–3483. <https://doi.org/10.1111/gcb.13623>
- Marin, M., Feng, M., Phillips, H. E., et al. (2021). A global, multiproduct analysis of coastal marine heatwaves: Distribution, characteristics, and long-term trends. *Journal of Geophysical Research: Oceans*, 126(2), e2020JC016708. <https://doi.org/10.1029/2020JC016708>
- Maturi, E., Harris, A., Mittaz, J., et al. (2017). A new high-resolution sea surface temperature blended analysis. *Bulletin of the American Meteorological Society*, 98(5), 1015–1026. <https://doi.org/10.1175/BAMS-D-15-00002.1>
- Mazzini, P., & Pianca, C. (2022). Marine heatwaves in the Chesapeake Bay. *Frontiers in Marine Science*, 8. <https://doi.org/10.3389/fmars.2021.750265>
- Met Office (2010 - 2015). Cartopy: A cartographic python library with a Matplotlib interface. Exeter, Devon. <https://scitools.org.uk/cartopy>
- Mills, K. E., Pershing, A. J., Brown, C. J., et al. (2013). Fisheries management in a changing climate: Lessons from the 2012 ocean heat wave in the Northwest Atlantic. *Oceanography*, 26(2), 191–195. <https://doi.org/10.5670/oceanog.2013.27>
- Mohamed, B., Nilsen, F., & Skogseth, R. (2022). Marine heatwaves characteristics in the Barents Sea based on high resolution satellite data (1982–2020). *Frontiers in Marine Science*, 9. <https://doi.org/10.3389/fmars.2022.821646>
- Oliver, E. (2023). Marine heatwaves. <https://github.com/ecjoliver/marineHeatWaves>
- Oliver, E. C. J., Burrows, M. T., Donat, M. G., et al. (2019). Projected marine heatwaves in the 21st century and the potential for ecological impact. *Frontiers in Marine Science*, 6. <https://doi.org/10.3389/fmars.2019.00734>
- Oliver, E. C. J., Donat, M. G., Burrows, M. T., et al. (2018). Longer and more frequent marine heatwaves over the past century. *Nature Communications*, 9(1), 1324. <https://doi.org/10.1038/s41467-018-03732-9>
- pandas development team T (2020). pandas-dev/pandas: Pandas. <https://doi.org/10.5281/zenodo.3509134>
- Pershing, A. J., Mills, K. E., Dayton, A. M., et al. (2018). Evidence for adaptation from the 2016 marine heatwave in the Northwest Atlantic Ocean. *Oceanography*, 31(2), 152–161. <https://doi.org/10.5670/oceanog.2018.213>
- Piccoloza, S., Toffolon, M., Robinson, C. T., et al. (2018). Exploring and quantifying river thermal response to heatwaves. *Water*, 10(8), 1098. <https://doi.org/10.3390/w10081098>
- Schlegel, R. W., Oliver, E. C. J., & Chen, K. (2021). Drivers of marine heatwaves in the Northwest Atlantic: The role of air-sea interaction during onset and decline. *Frontiers in Marine Science*, 8. <https://doi.org/10.3389/fmars.2021.627970>
- Schlegel, R. W., Oliver, E. C. J., Hobday, A. J., et al. (2019). Detecting marine heatwaves with sub-optimal data. *Frontiers in Marine Science*, 6, 737. <https://doi.org/10.3389/fmars.2019.00737>
- Shunk, N. P., Mazzini, P. L. F., & Walter, R. K. (2024). Impacts of marine heatwaves on subsurface temperatures and dissolved oxygen in the Chesapeake Bay. *Journal of Geophysical Research: Oceans*, 129(3), e2023JC020338. <https://doi.org/10.1029/2023JC020338>
- Smith, K. E., Burrows, M. T., Hobday, A. J., et al. (2021). Socioeconomic impacts of marine heatwaves: Global issues and opportunities. *Science*, 374(6566), eabj3593. <https://doi.org/10.1126/science.abj3593>
- Smith, K. E., Burrows, M. T., Hobday, A. J., et al. (2023). Biological impacts of marine heatwaves. *Annual Review of Marine Science*, 15(1), 119–145. <https://doi.org/10.1146/annurev-marine-032122-121437>
- Tassone, S. J., Besterman, A. F., Buelo, C. D., et al. (2022). Co-occurrence of aquatic heatwaves with atmospheric heatwaves, low dissolved oxygen, and low pH events in estuarine ecosystems.

- Estuaries and Coasts*, 45(3), 707–720. <https://doi.org/10.1007/s12237-021-01009-x>
- The Group for High Resolution Sea Surface Temperature Science Team, Piollé J. F., Armstrong, E., et al. (2022). The recommended GHSST data specification (GDS) (gds 2.1 revision 0). <https://doi.org/10.5281/zenodo.6984989>
- Tyrell, T. (2011). Anthropogenic modification of the oceans. *Philosophical Transactions of the Royal Society A*, 369, 887–908. <https://doi.org/10.1098/rsta.2010.0334>
- Virtanen, P., Gommers TERalf an Oliphant, Haberland M, et al. (2020). SciPy 1.0: Fundamental algorithms for scientific computing in python. *Nature Methods*, 17, 261–272. <https://doi.org/10.1038/s41592-019-0686-2>
- Wilks, D. S. (2016). “The stippling shows statistically significant grid points”: How research results are routinely overstated and over-interpreted, and what to do about it. *Bulletin of the American Meteorological Society*, 97(12), 2263–2273. <https://doi.org/10.1175/BAMS-D-15-00267.1>

Publisher's Note Springer Nature remains neutral with regard to jurisdictional claims in published maps and institutional affiliations.